Relationships between Cell Parameters of Dye-Sensitized Solar Cells and Dye-Adsorption Parameters

Puhong Wen,*,[†] Mei Xue,[§] Yoshie Ishikawa,[‡] Hiroshi Itoh,[‡] and Qi Feng*,[‡]

[†]Department of Chemistry and Chemical Engineering, Baoji University of Arts and Science, 1 Gaoxin Road, Baoji, Shaanxi 721013, P.R. China

[‡]Department of Advanced Materials Science, Faculty of Engineering, Kagawa University, 2217-20 Hayashi-cho, Takamatsu-shi 761-0396, Japan

[§]School of Chemistry and Chemical Engineering, Inner Mongolia University, 235 West University Road, Hohhot, 010021, P.R. China

Ⓢ *Supporting Information*

ABSTRACT: The performance of dye-sensitized solar cells (DSCs) is affected strongly by sensitizer-dye adsorption behavior on TiO_2 nanocrystal electrode. This study reports quantitative relationships between DSC cell performance parameters and dye-adsorption parameters for the first time. We discovered a logarithmic relationship between short-circuit photocurrent density (J_{sc}) and dye-adsorption equilibrium constant on TiO_2 surface, and a linear relationship between open-circuit potential (V_{oc}) and dye-adsorption density on TiO_2 surface for DSCs. These relationships provide a convenient method for forecasting the performance of TiO_2 nanoparticles for DSCs from the dye-adsorption parameters, and also indicate future directions for the development of high-performance TiO_2 nanoparticles for DSCs.

KEYWORDS: *dye-sensitized solar cell, cell performance, dye-adsorption, photocurrent, photovoltage*
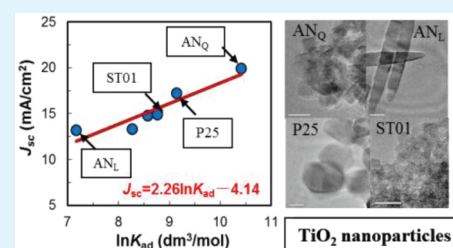
1. INTRODUCTION

The DSCs are the promising candidates for photovoltaic power generation because of their low manufacturing cost and relatively high power-conversion efficiency.[1] A typical DSC consists of a dye-adsorbed mesoporous TiO_2 nanoparticle film electrode, a Pt counter-electrode, and an electrolyte solution containing a tri-iodide/iodide redox couple between the electrodes. The immobilized dye absorbs a photon to produce an excited state, which transfers efficiently its electron onto the TiO_2 conduction band. The oxidized dye is subsequently reduced by electron donation from the electrolyte containing the tri-iodide/iodide system. The injected electron flows through the semiconductor network to arrive at the back contact and then through the external load to the counter-electrode. At the counter-electrode, reduction of tri-iodide in turn regenerates iodide, which completes the circuit. Unlike physical solar cells, such as silicon solar cells, the DSCs are chemical solar cells, and the charge transfer processes are complex. Therefore, many factors, such as TiO_2 nanocrystals,[2] sensitizers,[3] redox electrolytes,[4] electric additives,[5] etc., can influence the DSC performance. To analyze the performance of each part of a DSC, the fabrication of DSCs with good repeatability is necessary. However, great skill and know-how are required for DSC fabrication, though it does not require expensive equipments.[6]

The TiO_2 electrode is the most significant part of a DSC, and its performances strongly depend on dye-adsorption on the TiO_2 nanocrystal surface. For this reason, a large number of studies have been reported on the preparation of TiO_2 nanocrystals. However, most of these crystals have not been characterized as material for the TiO_2 electrode because the fabrication of DSCs for the characterization is a hard work and the results have low repeatability. It has been realized that dye-adsorption is important for enhancing DSCs performance, and some studies have reported on the dye-adsorption. Adachi et al. have prepared a single-crystalline anatase exposing mainly the {101} plane, which adsorbed ruthenium dye over 4 times higher as compared to P25.[7] Neal et al. have investigated the effect of a chenodeoxycholate coadsorbent on the performance of DSCs, and revealed that the chenodeoxycholate adsorption reduces the dye loading by as much as 60% while having a relatively small influence on the short-circuit photocurrent by photocurrent−voltage measurements combined with desorption studies.[8] Most of these studies have focused mainly on the adsorption amount to increase the photoabsorption. Although the adsorption equilibrium constant is another important parameter of the adsorption reaction, no studies have reported on this parameter until our recent study.[9] These results suggest that both of the dye adsorption amount and the dye adsorption equilibrium constant on the TiO_2 nanoparticles affect the performance of DSCs.

The prevalent method for appraising TiO_2 nanoparticles performance in DSCs is fabrication of DSCs using the TiO_2 nanoparticles, and then measurement of the cell parameters of the fabricated DSCs. Because there are the many factors impacting performance of DSCs in the fabricating process, it is not easy to fabricate good repeatability DSCs. Here we report quantitative relationships between DSC performance parameters and dye-adsorption parameters, and give a convenient method to forecast the performance of TiO_2 nanoparticles for DSCs from the dye-adsorption parameters.

2. MATERIALS AND METHODS

2.1. Chemicals and Reagents. Ten weight percent tetrabutylammonium hydroxide (TBAOH) aqueous solution, n-propylamine (PA) solution, and 20 wt % poly(diallyldimethylammoniumchloride) (PDDA-Cl, M_w = 2.0 × 10^5 to 3.5 × 10^5) aqueous solution were purchased from Tokyo chemicals. N719 (cis-di(thiocyanate)bis(2,2′-bipyridyl-4,4′-dicarboxylate)-ruthenium(II) bis-tetrabutylammonium) was purchased from Sigma-Aldrich. P25 (commercial TiO_2 powder) was obtained from Degussa. ST01 (commercial TiO_2 powder) was obtained from Ishihara. ST111 (commercial TiO_2 powder) was obtained from Titan Kogyo. Other chemicals and reagents were of analytical grade, and all the reagents were used as received without further purification.

2.2. Synthesis of TiO_2 Nanocrystals. To prepare anatase samples AN_Q, AN_L, AN_C, and AN_R, we treated a layered titanate ($H_{1.07}Ti_{1.73}O_4$) with lepidocrocite-like structure in a TBAOH solution or a PA solution to exfoliate the layered titanate into its nanosheets. The titanate nanosheet solution was then reacted under hydrothermal conditions.[10,11] The AN_Q and AN_C were obtained by hydrothermal reaction of a titanate nanosheet solution of TBAOH at 120 °C and pH 1.8, and at 100 °C and pH 11.5, respectively. The sample AN_L was obtained by hydrothermal reaction of a titanate nanosheet solution of PA at 135 °C and pH 11.3. The sample AN_R was obtained by hydrothermal reaction of a nanocomposite slurry solution at 150 °C and pH 9.2. The nanocomposite slurry solution was obtained by slowly dropping PDDA-Cl solution with monomer concentrations of 3.0 × 10^{-2} mol/L into the titanate nanosheet solution of PA under stirring condition at room temperature.[11,12]

2.3. Dye Adsorption Experiment. A TiO_2 powder sample (10 mg) was added to an ethanol solution (5 mL) of N719 dye in a concentration range of 1.0 × 10^{-4} to 1.0 × 10^{-3} mol/L, and the mixture was then stirred at room temperature for 72 h. The concentrations of N719 dye before and after adsorption were measured using a SHIMADZU UV-2450 spectrophotometer. The TiO_2 powder sample was calcined at 450 °C for 30 min before the adsorption experiment.

2.4. Fabrication of DSC. A TiO_2 film electrode was prepared by the doctor-blade technique, using TiO_2 nanocrystal paste on an FTO glass plate (25 × 25 mm). The paste sample was prepared by dispersing TiO_2 nanocrystals sample in a 0.2 mol/L HNO_3 solution containing 3wt.% of Triton X-100, 5wt.% of acetylacetone, and 10 wt % of polyethylene glycol (PEG) (molecular weight of 20 000). The TiO_2 content in the paste was adjusted to about 15−18 wt % to control the thickness of the TiO_2 film. After being coated with the paste on the FTO glass plate, the TiO_2 film electrode was calcined at 450 °C for 30 min and then immersed into a 3 × 10^{-4} mol/L N719 dye solution in a mixed solvent of acetonitrile and tert-butyl alcohol (1:1 volume ratio) for 24 h to adsorb the dye onto the TiO_2 electrode. The DSC was comprised of the dye-adsorbed TiO_2 electrode and a Pt-coated conducting glass counter-electrode, with an electrolyte solution between the electrodes. The electrolyte solution contained butylmethylimidazolium iodide (0.60 mol/L), I_2 (0.03 mol/L), guanidinium thiocyanate (0.10 mol/L), and 4-tert-butylpyridine (0.50 mol/L) in a mixed solvent of acetonitrile and valeronitrile (85%:15% volume ratio).

2.5. Dye Desorption from TiO_2 Electrode. Two parallel TiO_2 film electrodes were prepared for each TiO_2 nanoparticle sample in the dye desorption experiment. After being calcined at 450 °C for 30 min, one was immersed into the 3 × 10^{-4} mol/L N719 dye solution in the mixed solvent of acetonitrile and tert-butyl alcohol (1:1 volume ratio) at room temperature for 72 h to adsorb the dye onto the TiO_2 film electrode, and another was used as the blank sample. And then the dye-adsorbed electrode was immersed into an ethanol solution at room temperature for 72 h to desorb the dye. The amounts of the dye adsorbed on the film before and after the dye-desorption treatment were measured by the spectrophotometer with the blank sample as reference. The percentage of the desorbed dye was evaluated from ratio of absorbance before and after desorbing.

2.6. Characterizations of DSCs and Materials. The photocurrent−voltage characteristic curves for the DSCs were measured using a Hokuto-Denko BAS100B electrochemical analyzer under irradiation with simulated sunlight of AM 1.5 (100mW/cm^2), using a sunlight simulator (YSS-E40, Yamashita Denso) and a 0.25 cm^2 mask. TEM observation was performed on a JEOL JEM-3010 at 300 kV with the sample supported on a microgrid. Powder X-ray diffraction (XRD) analysis of the samples was carried out on a SHIMADZU XRD-6100 X-ray diffractometer with Cu Kα (λ = 0.15418 nm) radiation. Nitrogen gas adsorption was carried out on a QUANTACHROME AUTOSORB-1-MP apparatus. The specific surface area was calculated from the adsorption data using the Brunauer−Emmett−Teller (BET) method. The thicknesses of the TiO_2 films were measured using a SURFCOM 480A surface-shape determiner.

3. RESULTS AND DISCUSSION

3.1. Characterizations of TiO_2 Nanocrystals. Factors involving the specific surface area, the lattice plane on the crystal surface, the crystal morphology, and the crystallinity of the TiO_2 nanocrystals are expected to affect the dye adsorption parameters. To investigate the relationships between DSC performance parameters of J_{sc} and V_{oc} and the dye adsorption parameters, we choose seven kinds of TiO_2 nanocrystal samples with different crystal sizes, crystal morphologies, and lattice planes on the crystal surface. Three are typical commercial TiO_2 nanocrystal samples, ST01, ST111, and P25, with different crystal sizes. An XRD study indicated that P25 is mixed phases of anatase (80%) and rutile (20%), and other are single phase of anatase as shown in Figure 1a. The width and acutance of diffraction peaks indicate the crystallinity increasing order of ST01 < ST111 < P25. Transmission electron microscopy (TEM) images of these TiO_2 nanocrystals are present in Figure 2. The ST01 and ST111 samples have spherical crystal morphologies with sizes of about 7 nm (ST01) and 10 nm (ST111). The P25 sample has a cubic morphology with a crystal size of about 30 nm.

Four self-prepared anatase nanocrystal samples with different crystal morphologies, AN_Q, AN_L, AN_C, and AN_R, are prepared from exfoliated layered titanate ($H_{1.07}Ti_{1.73}O_4$) nanosheet solutions by hydrothermal reactions.[10−12] Figure 1b shows the XRD patterns of AN_Q, AN_L, AN_C, and AN_R samples. The results indicate that these four samples are single phase of anatase and the crystallinity increases in an order of AN_Q < AN_C < AN_L < AN_R. Figure 2D−H presents TEM (E, G, and H) and high-resolution transmission electron microscopy (HRTEM, D and F) images of these TiO_2 nanocrystals. The AN_Q, AN_L, AN_C, and AN_R samples have quadrate, nanoleaf-like, nanocomb-like, and nanorod-like crystal morphologies, respectively. The HRTEM images indicate that the sides of the quadrate nanoparticles correspond to (100) and (001) planes, respectively, and therefore the basal plane corresponds to (010) plane. In the nanoleaf-like particles, the basal plane also corresponds to (010) plane, and the axis-direction corresponds to the [001] direction. Similar to the quadrate and nanoleaf-like
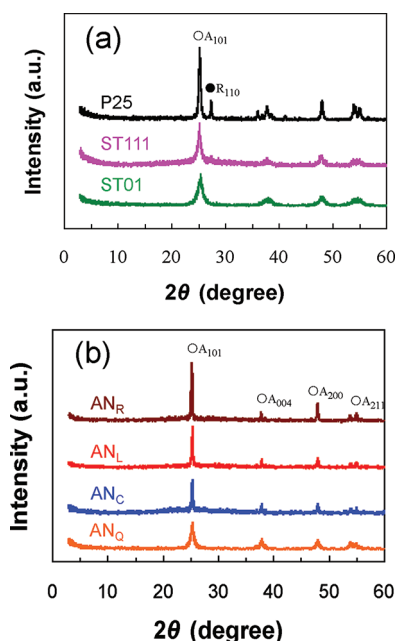
Figure 1. XRD patterns of (a) commercial TiO$_2$ nanocrystal samples and (b) self-prepared TiO$_2$ nanocrystal samples.

Figure 2. TEM and HRTEM images of TiO$_2$ nanocrystals used in this study. (A) ST01, (B) ST111, and (C) P25 are commercial TiO$_2$ nanocrystal samples. (D) AN$_Q$, (E, F) AN$_L$, (G) AN$_C$, and (H) AN$_R$ are locally prepared TiO$_2$ nanocrystal samples. The HRTEM images D and F indicate that the locally prepared TiO$_2$ nanocrystals preferentially exhibit the (010) lattice plane on the crystal surface.

particles, the basal planes of nanocomb-like and nanorod-like particles also correspond to (010) plane because these nanoparticles are formed by topotactic structural transformation reaction from the layered titanate nanosheets.[10−12] These results reveal that the quadrate, nanoleaf-like, nanocomb-like, and nanorod-like particles preferentially exhibit the (010) plane on their particles surface.

The average crystallite dimensions of anatase nanocrystals in [004], [200], and [010] directions can be estimated from the average crystallite sizes calculated from the full width at half-maximum (fwhm) of XRD diffraction peaks of (004), (200), and (211), respectively, by using the Sherrer formula.[10,13] The results suggest that the quadrate, nanoleaf-like, nanocomb-like, and nanorod-like particles have average crystallite sizes of about 20 × 10 × 15 nm, 40 × 20 × 300 nm, 150 × 10 × 300 nm, and 60 × 60 × 500 nm in [200] × [010] × [004] dimensions, respectively (see the Supporting Information). On the basis of the results, we estimate the percentage of {010} facets exposed on the AN$_Q$ and AN$_L$ particles surfaces as about 63 and 48%, respectively.

3.2. Dye adsorption on TiO$_2$ Nanocrystals. A typical sensitizer dye used in DSCs, N719 is used in the dye-adsorption experiment carried out by a batch method. Figure 3 presents the dependencies of the dye uptake amount on the concentration of the dye, i.e., the adsorption isotherms, for these seven TiO$_2$ nanocrystal samples. The TiO$_2$ samples used in this study have quite different Brunauer−Emmett−Teller (BET) specific surface areas (S_{BET}) (Table 1), and the dye uptake amounts of the per gram sample strongly depend on S_{BET}. To more clearly understand the situation of the dye molecules adsorbed on the crystal surface, we present the dye uptake amount as per S_{BET} of the sample that corresponds to dye adsorption density on the crystal surface (mol/m^2). The experimental data for the dye adsorption fit the Langmuir isotherm for all of these samples, indicating Langmuir monolayer adsorption on the TiO$_2$ nanocrystals.[11] The
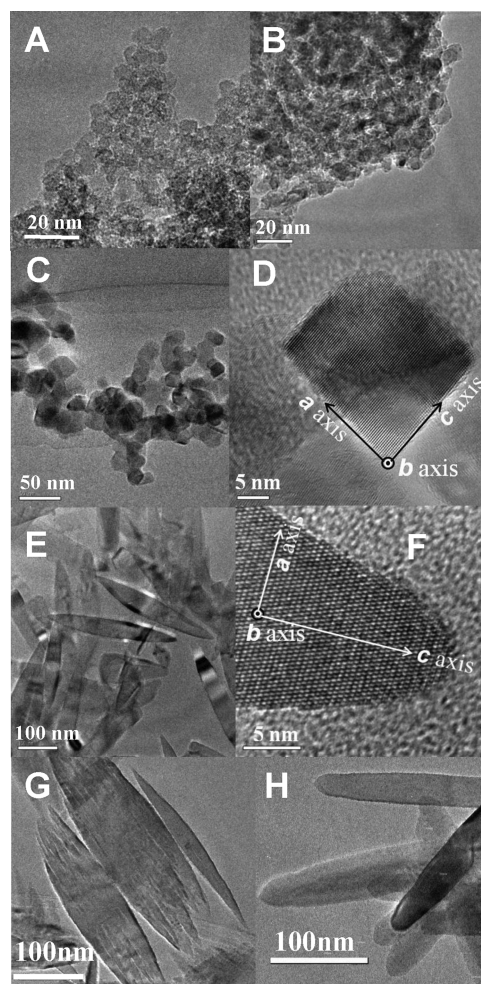
Langmuir equation can be represented by the following linear formula

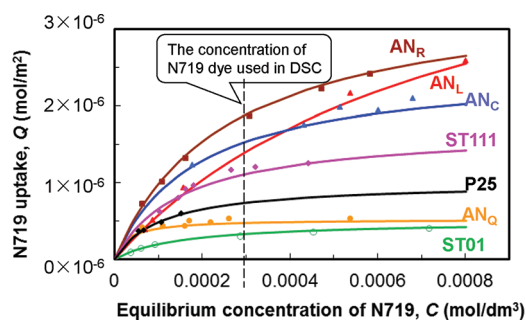$$C/Q = 1/(Q_mK_{ad}) + C/Q_m \qquad (1)$$

Figure 3. Adsorption isotherms for N719 dye on TiO$_2$ nanocrystal samples of AN$_R$, AN$_L$, AN$_C$, ST111, P25, AN$_Q$, and ST01. The markers correspond to the experiment data, and the lines, to the fitting to the Langmuir equation. The square correlation coefficients of the fitting are 0.998 for AN$_R$, 0.962 for AN$_L$, 0.991 for AN$_C$, 0.960 for ST111, 0.953 for P25, 0.972 for AN$_Q$, and 0.994 for ST01.

1930

dx.doi.org/10.1021/am3001693 | ACS Appl. Mater. Interfaces 2012, 4, 1928−1934

Table 1. Surface Area and N719 Dye-Adsorption Parameters of the TiO$_2$ Nanocrystals, And Cell Parameters of DSCs Fabricated Using the TiO$_2$ Nanocrystals

sample	S_{BET} (m^2/g)	K_{ad} (dm^3/mol)	Q_m (mol/m^2)	$Q_{0.3}$ (mol/m^2)	$Q_{0.3}$ (molecule/nm^2)	V_{oc} (V)	J_{sc} (mA/cm^2)	ff	η (%)
ST01	349	6400	5.0×10^{-7}	3.3×10^{-7}	0.2	0.651	14.9	0.54	5.3
ST111	312	6400	1.7×10^{-6}	1.1×10^{-6}	0.7	0.674	15.2	0.51	5.2
P25	63	9300	1.0×10^{-6}	7.4×10^{-7}	0.4	0.669	17.2	0.55	6.3
AN$_Q$	131	33300	5.0×10^{-7}	4.6×10^{-7}	0.3	0.637	19.9	0.43	5.4
AN$_C$	46	5300	2.5×10^{-6}	1.5×10^{-6}	0.9	0.725	14.8	0.54	5.6
AN$_L$	35	1300	5.0×10^{-6}	1.4×10^{-6}	0.8	0.717	13.2	0.61	5.8
AN$_R$	32	3900	3.5×10^{-6}	1.9×10^{-6}	1.1	0.746	13.3	0.57	5.6

where Q is the N719 uptake density (mol/m^2), and C is the equilibrium concentration of N719 in the solution (mol/dm^3). From the fitting of the experimental data to the Langmuir equation (eq 1) by plotting C/Q against C, the saturation (maximum) adsorption density Q_m (mol/m^2) and the adsorption equilibrium constant K_{ad} (dm^3/mol) for N719 onto the samples were evaluated as given in Table 1. The adsorption equilibrium constant is a thermodynamic equilibrium constant, corresponding to the binding energy of the adsorption. The N719 uptake density $Q_{0.3}$ at a concentration of 0.3 mmol/L is also listed in Table 1 because the 0.3 mmol/L N719 solution is used for the adsorption of the dye on the TiO$_2$-electrode in the DSC fabrication process. These seven TiO$_2$ nanocrystals exhibit significant differences in N719 adsorption. Q_m grows in the order of ST01=AN$_Q$ < P25 < ST111 < AN$_C$ < AN$_R$ < AN$_L$, while the value of K_{ad} increases in the order of AN$_L$ < AN$_R$ < AN$_C$ < ST01 = ST111 < P25 < AN$_Q$. These results indicate that the adsorption binding of the dye to the AN$_Q$ crystal surface is the strongest, and that the density of the dye adsorbed on the AN$_L$ crystal surface is the highest under saturation adsorption conditions. The different Q_m and K_{ad} values may be due to differing amounts of adsorption sites and different adsorption binding configurations of the dye molecules on the TiO$_2$ nanocrystals,[14,15] which have different lattice planes on their surfaces and different morphologies.

3.3. Current−Voltage Characteristic Curves for DSCs.
To study the DSCs performance of the TiO$_2$ nanocrystals, we fabricate DSCs using these seven TiO$_2$ nanocrystal samples. In the DSC fabrication, 0.3 mmol/L N719 dye solution is using for the dye adsorption. It has been reported that TiO$_2$ film thickness affects the DSC performance.[6,8,16] Thicker TiO$_2$ film adsorbs more dye and increase the current density. But accompanying both increase of the recombination loss of injected electrons in TiO$_2$ film and the increase in series resistance of DSC can limit continuous increase of current density.[16] Open-circuit voltages of the DSCs decrease with an increase of the film thickness. The decrease of the open-circuit voltage is explained as a consequence of increased charge recombination and restricted mass transport in thicker films.[6] In the present study, the effects of the film thickness on V_{oc} and J_{sc} are showed in Figure S1 in the Supporting Information. For most of samples, the V_{oc} slightly decreases by increasing the film thickness, but the decrease is small (about 3%) in the thickness region of 8 to 13 μm, which can be ignored. The J_{sc} increases with the film thickness up to 8 μm, and then keeps almost constant in the thickness region of 8 to 13 μm. These results suggest that the relatively smaller variations of the V_{oc} and J_{sc} values can be obtained in the thickness region of 8−13 μm. Therefore, the thickness of the TiO$_2$ film is controlled in a

region of 9−12 μm for the characterization in order to reduce the experimental errors, except for the AN$_Q$ sample (6 μm), which has the highest J_{sc} value.

Typical current−voltage characteristic curves for AN$_R$-based, AN$_L$-based, AN$_C$-based, AN$_Q$-based, P25-based, ST01-based, and ST111-based DSCs are presented in Figure 4. Photovoltaic
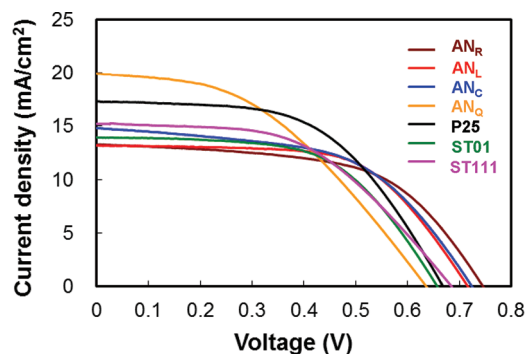

Figure 4. Photocurrent−voltage characteristic curves of DSCs prepared using the TiO$_2$ nanocrystal samples of AN$_R$, AN$_L$, AN$_C$, AN$_Q$, P25, ST01, and ST111. The photovoltaic parameters of V_{oc}, J_{sc}, ff, and η for the DSCs in Table 1 were evaluated from the current−voltage curves.

parameters of the short-circuit photocurrent density (J_{sc}), the open-circuit potential (V_{oc}), the fill factor (ff), and the power-conversion efficiency (η) for the DSCs prepared by using the TiO$_2$ nanocrystals described above are summarized in Table 1. These cell parameters were evaluated from the current−voltage curves of the DSCs in Figure 4. These samples exhibit a variety of the cell performance, and the AN$_R$ sample has the highest V_{oc} value, and the AN$_Q$ sample has the highest J_{sc} value than that of the others samples.

3.4. Relationships between the Cell Parameters and the Adsorption Parameters.
It is very interesting that the J_{sc} increasing order of AN$_L$ < AN$_R$ < AN$_C$ < ST01 < ST111 < P25 < AN$_Q$ agrees with the K_{ad} increasing order of AN$_L$ < AN$_R$ < AN$_C$ < ST01=ST111 < P25 < AN$_Q$, and the increasing order of V_{oc} AN$_Q$ < ST01 < P25 < ST111 < AN$_L$ < AN$_C$ < AN$_R$ is almost the same as the $Q_{0.3}$ increasing order of ST01 < AN$_Q$ < P25 < ST111 < AN$_L$ < AN$_C$ < AN$_R$, except for the AN$_Q$ sample. To determine the quantificational relationships between the cell parameters and the adsorption parameters, we plot J_{sc} against K_{ad}, and V_{oc} against $Q_{0.3}$ (Figure 5). The curve of J_{sc} against K_{ad} reveals a logarithmic relationship. For using expediently, we plot J_{sc} against lnK_{ad}, and then a logarithmic relationship of J_{sc} = 2.26lnK_{ad}−4.14 with a correlation coefficient of 0.936 and a relative average deviation of 4.8% is obtained for J_{sc} and K_{ad}. A linear relationship of V_{oc} = 6.80 × 10$^4Q_{0.3}$+0.616 with a
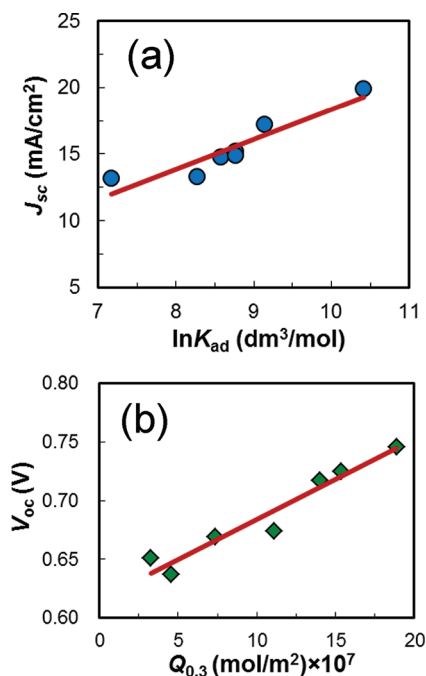
Figure 5. Relationship between the cell parameters and the dye-adsorption parameters. (a) Relationship between the short-circuit photocurrent density (J_{sc}) and the dye-adsorption equilibrium constant (K_{ad}) ($J_{sc} = 2.26\ln K_{ad} - 4.14$). (b) Relationship between the open-circuit potential (V_{oc}) and the dye uptake amount ($Q_{0.3}$) in 0.3 mmol/L N719 dye solution ($V_{oc} = 6.80 \times 10^4 Q_{0.3} + 0.616$). DSCs were prepared using AN_R, AN_L, AN_C, ST111, P25, AN_Q, and ST01 TiO_2 nanocrystal samples.

correlation coefficient of 0.968 and a relative average deviation of 1.2% is obtained for V_{oc} and $Q_{0.3}$. These relationships also suggest that the dye-adsorption results of the TiO_2 nanoparticles can be used to estimate the dye-adsorption behavior in the network of TiO_2-film electrode, namely the TiO_2 nanoparticles keep their dye-adsorption characteristics in the network of TiO_2-film electrode.

The increase in the adsorption equilibrium constant K_{ad} suggests the enhancement of binding strength of the dye on TiO_2 surface. The experiment results of N719 dye-desorption from the TiO_2-films support this idea, as shown in Figure 6. The N719 desorption percentage from TiO_2-films in ethanol solution increases in the order of AN_Q < ST111 < AN_L, which agrees with the decreasing order of K_{ad} AN_Q > ST111 > AN_L; indicating the dye-adsorption is stronger on the TiO_2 nanocrystal surface that has larger K_{ad} value. The increase in J_{sc} with increasing the adsorption equilibrium constant K_{ad}
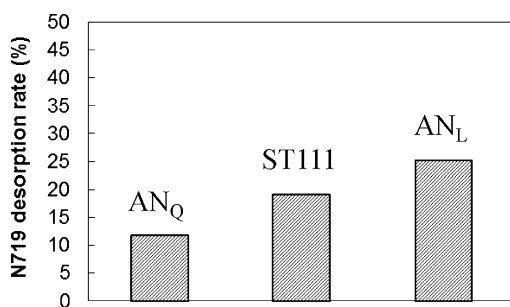

Figure 6. Desorption of N719 dye from TiO_2-films in ethanol solution at room temperature for 72 h.

suggests that strong anchoring of the dye molecule onto the TiO_2 surface can enhance J_{sc}. The strong anchoring can accelerate the injection rate of excited photoelectrons from the dye molecule into the TiO_2 surface.[8,9] An UV−vis spectrum study indicates that N719 dye spectrum presents a red-shift after adsorbing on TiO_2 surface, and the red-shift is larger for AN_Q sample that has larger K_{ad} than that of AN_L that has smaller K_{ad} (see Figure S2 in the Supporting Information). The red-shift can enhance the absorption wavelength region of visible light that would enhance also J_{sc}.

The increase in the V_{oc} value with increasing dye uptake density can be explained by reduced charge recombination at the TiO_2/electrolyte interface. The high density of the dye adsorbed onto the TiO_2 electrode surface can insulate the TiO_2 surface from the electrolyte, which decreases electron transfer from the TiO_2 surface to I_3^- ions in the electrolyte (charge recombination) and causes an increase in V_{oc}.[17] Similar effect has also been observed when a coadsorbent of the dye was used.[18] We also estimate how many N719 molecules are adsorbed in per nm^2 (molecule/nm^2) from the adsorption density result of mol/m^2 in the TiO_2-films of DSCs fabricated using 0.3 mmol/L N719 solution, as shown in Table 1. It has been reported that in the N719 molecule ([Ru-(dcbpy)$_2$(NCS)$_2$](TBA)$_2$), the molecular diameter of [Ru-(dcbpy)$_2$(NCS)$_2$]$^{2-}$ ion is about 1 nm.[14,19] Therefore, almost all (100%) of TiO_2 surface is covered by the dye molecules in the AN_R-based TiO_2-film, whereas only 20% of the surface is covered by the dye molecules in the ST01-based TiO_2-film by assuming the monolayer dye-adsorption. These results reveal that there is much open space on ST01-based (80%), AN_Q-based (70%), and P25-based (50%) TiO_2 electrodes surface, where without adsorbed dye and the TiO_2 surface contacts directly with the electrolyte solution. The open space causes the charge recombination at the TiO_2/electrolyte interface. This is the reason why these nanoparticles exhibit the lower V_{oc} values. On the other hand, there is little open space on AN_R-based (0%), AN_C-based (10%), and AN_L-based (20%) TiO_2-electrodes surface, and these nanoparticles exhibit the higher V_{oc} values.

We also found that the *ff* increasing order of AN_Q < ST111 < ST01 = AN_C < P25 < AN_R < AN_L is different from the $Q_{0.3}$ increasing order of ST01 < AN_Q < P25 < ST111 < AN_L < AN_C < AN_R, although suppressing the charge recombination could increase *ff* as well.[20] This suggests that *ff* is also affected by other factors that are independent of the dye-adsorption. One of the important factors is the conductivity of the TiO_2 film. It has been reported that increasing the conductivity of TiO_2 film by adding one-dimensional nanowire-like particles into the spherical nanoparticles can enhance the *ff* value.[21,22]

In the present study, the AN_Q sample had the highest J_{sc} value of 19.9 mA/cm^2, and the AN_R sample had the highest V_{oc} of 0.746 V, whereas P25 sample gave the highest η of 6.3%. This result indicates that it is necessary to design a high-performance TiO_2 nanocrystal with large adsorption equilibrium constant and high dye-adsorption density on the surface in order to develop a high-performance DSC. However, the large adsorption equilibrium constant that determines J_{sc} would be more important than the dye-adsorption density that affects V_{oc} because in addition to increasing the dye-adsorption density, V_{oc} can also be enhanced by other surface-modification techniques, such as using a coadsorbent[17] or electric additives.[5] Therefore, we think AN_Q with highest J_{sc} value is a promising TiO_2 nanoparticle sample for high performance DSCs. In order

1932

dx.doi.org/10.1021/am3001693 | *ACS Appl. Mater. Interfaces* 2012, 4, 1928−1934

to demonstrate the performance of AN_Q sample, we mixed the leaf-like AN_L (20%) with AN_Q (80%). Figure 7 shows the
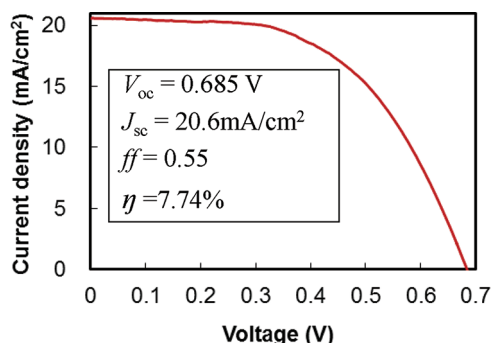

Figure 7. Photocurrent—voltage characteristic curve of DSC prepared using the TiO$_2$ nanocrystal sample mixed by AN_Q (80%) and AN_L (20%).

photocurrent—voltage characteristic curve of DSC prepared using the AN_Q-AN_L mixed sample. The cell parameters of V_{oc}, J_{sc}, ff, and η for the DSC enhance 8, 4, 28, and 43%, respectively, comparing with which for original AN_Q-based DSC. And the η value (7.7%) is also much higher than that of P25-based DSC (6.3%). The main reasons of the enhanced cell parameters are that the addition of the one-dimensional leaf-like particles can be effective to increase the conductivity for transferring the photoelectrons from the TiO$_2$ film to FTO glass surface that decreases the recombination loss of injected electrons in TiO$_2$ film and enhances the V_{oc} and ff,[23] and the relatively larger particle size of AN_L also causes the light-trapping effect that enhances the J_{sc}.[24]

The results of the present study suggest that the lattice plane on the surface and the morphology of the nanocrystals are essential factors for enhancing the adsorption equilibrium constant and the adsorption density. For designing a high-performance dye molecule, in addition to its photoabsorption properties, strong anchoring onto the TiO$_2$ surface is necessary. Increasing the anchoring groups (typically carboxylic acid —COOH) available to the TiO$_2$ surface in each dye molecule would be effective in enhancing the anchoring strength. In fact, most excellent Ru complex dyes have two or more anchoring carboxyl groups.[25]

4. CONCLUSION

In the present study, we have demonstrated the logarithmic relationship between J_{sc}, and the dye-adsorption equilibrium constant and the linear relationship between V_{oc} and the dye-adsorption amount for DSC. These relationships provide a new method for forecasting the cell parameters and cell features based on the dye-adsorption parameters by comparing the parameters with a standard TiO$_2$ nanocrystal sample, such as P25. Because adsorption parameters are easily measured with relatively higher repeatability, it is a convenient and low-cost method for characterizing DSC features. These relationships have also yielded useful information for developing high-performance TiO$_2$ nanocrystals, dyes, and DSCs.

ASSOCIATED CONTENT

Ⓢ Supporting Information
Estimating average crystallite dimensions of anatase nanocrystals, dependences of the DSC cell performance on the TiO$_2$ film thickness, and the absorbing spectra of N719 adsorb-binding on

the surface of AN_L and AN_Q samples. This material is available free of charge via the Internet at http://pubs.acs.org.

AUTHOR INFORMATION

Corresponding Author
*E-mail: feng@eng.kagawa-u.ac.jp.

Notes
The authors declare no competing financial interest.

ACKNOWLEDGMENTS

REFERENCES

(1) Nazeeruddin, M. K.; DeAngelis, F.; Fantacci, S.; Sellon, A.; Viscardi, G.; Liska, P.; Ito, S.; Takeru, B.; Grätzel, M. *J. Am. Chem. Soc.* **2005**, *127*, 16835−16847.
(2) Tamotsu, H.; Hidetoshi, M.; Kouichi, S.; Satoshi, U. *J. Am. Chem. Soc.* **2004**, *126*, 12218−12219.
(3) Song, J.; Zhang, F.; Li, C.; Liu, W.; Li, B.; Huang, Y.; Bo, Z. *J. Phys. Chem. C* **2009**, *113*, 13391−13397.
(4) Wang, P.; Zakeeruddin, S. M.; Moser, J. E.; Baker, R. H.; Grätzel, M. *J. Am. Chem. Soc.* **2004**, *126*, 7164−7165.
(5) Dürr, M.; Yasuda, A.; Nelles, G. *Appl. Phys. Lett.* **2006**, *89*, 061110−1−3.
(6) Tan, B.; Wu, Y. *J. Phys. Chem. B* **2006**, *110*, 15932−15938.
(7) Adachi, M.; Murata, Y.; Takao, J.; Jui, J.; Sakamoto, M.; Wang, F. *J. Am. Chem. Soc.* **2004**, *126*, 14943−14949.
(8) Neal, N. R.; Kopidakis, N.; van de Lagemaat, J.; Grätzel, M.; Frank, A. J. *J. Phys. Chem. B* **2005**, *109*, 23183−23189.
(9) Wen, P.; Tao, Z.; Ishikawa, Y.; Itoh, H.; Feng, Q. *Appl. Phys. Lett.* **2010**, *97*, 131906−1−3.
(10) Wen, P.; Itoh, H.; Tang, W.; Feng, Q. *Langmuir* **2007**, *23*, 11782−11790.
(11) Wen, P.; Itoh, H.; Tang, W.; Feng, Q. *Microporous Mesoporous Mater.* **2008**, *116*, 147−156.
(12) Wen, P.; Ishikawa, Y.; Itoh, H.; Feng, Q. *J. Phys. Chem. C* **2009**, *113*, 20275−20280.
(13) Wu, B.; Guo, C.; Zheng, N.; Xie, Z.; Galen, D. S. *J. Am. Chem. Soc.* **2008**, *130*, 17563−17567.
(14) Zuleta, M.; Yu, S.; Ahmadi, S.; Boschloo, G.; Gothelid, M.; Hagfeldt, A. *Langmuir* **2010**, *26*, 13236−13244.
(15) Lee, K. E.; Gomez, M. A.; Elouatik, S.; Demopoulos, G. P. *Langmuir* **2010**, *26*, 9575−9583.
(16) Murayama, M.; Mori, T. *Thin Solid Films* **2008**, *516*, 27162−2722.
(17) Meng, Q. B.; Takahashi, K.; Zhang, X. T.; Sutanto, I; Rao, T. N.; Sato, O.; Fujishima, A.; Watanabe, H.; Nakamori, T.; Uragami, M. *Langmuir* **2003**, *19*, 3572−3574.
(18) Zhang, Z.; Evans, N.; Zakeeruddin, S. M.; Humphry-Baker, R.; Grätzel, M. *J. Phys. Chem. C* **2007**, *111*, 398−403.
(19) Katoh, R.; Kasuya, M.; Furube, A.; Fuke, N.; Koide, N.; Han, L. *Chem. Phys. Lett.* **2009**, *471*, 280−282.
(20) Zhao, N.; Osedach, T. P.; Chang, L.-Y.; Geyer, S. M.; Wanger, D.; Binda, M. T.; Arango, A. C.; Bawendi, M. G.; Bulovic, V. *Nano* **2010**, *4*, 3743−3752.
(21) Kang, S. H.; Choi, S.-H.; Kang, M.-S.; Kim, J.-Y.; Kim, H.-S.; Hyeon, T.; Sung, Y.-E. *Adv. Mater.* **2008**, *20*, 54−58.

(22) Tang, Y.-B.; Lee, C.-S.; Xu, J.; Liu, Z.-T.; Chen, Z.-H.; He, Z.; Cao, Y.-L.; Yuan, G.; Song, H.; Chen, L.; Luo, L.; Cheng, H.-M.; Zhang, W.-J.; Bello, I.; Lee, S.-T. *Nano* **2010**, *4*, 3482−3488.

(23) Usami, A. *Sol. Energy Mater. Sol. Cells* **2000**, *64*, 73−83.

(24) Tachibana, Y.; Hara, K.; Sayama, K.; Arakawa, H. *Chem. Mater.* **2002**, *14*, 2527−2535.

(25) Hara, K.; Sugihara, H.; Tachibana, Y.; Islam, A.; Yanagida, M.; Sayama, K.; Arakawa, H. *Langmuir* **2001**, *17*, 5992−5999.